First Principles Analysis of H2O Adsorption on the (110) Surfaces of SnO2, TiO2 and Their Solid Solutions

Hahn, Konstanze R ; Tricoli, Antonio ; Santarossa, Gianluca ; Vargas, Angelo ; Baiker, Alfons

Abstract: Both associative and dissociative H2O adsorption on SnO2(110), TiO2(110), and Ti-enriched Sn1-xTixO2(110) surfaces have been investigated at low (1/12 monolayer (ML)) and high coverage (1 ML) by density functional theory calculations using the Gaussian and plane waves formalism. The use of a large supercell allowed the simulation at low symmetry levels. On SnO2(110), dissociative adsorption was favored at all coverages and was accompanied by stable associative H2O configurations. Increasing the coverage from 1/12 to 1 ML stabilized the (associatively or dissociatively) adsorbed H2O on SnO2(110) because of the formation of intermolecular H bonds. In contrast, on TiO2(110), the adsorption of isolated H2O groups (1/12 ML) was more stable than at high coverage, and the favored adsorption changed from dissociative to associative with increasing coverage. For dissociative H2O adsorption on Ti-enriched Sn1-xTixO2(110) surfaces with Ti atoms preferably located on 6-fold-coordinated surface sites, the analysis of the Wannier centers showed a polarization of electrons surrounding bridging O atoms that were bound simultaneously to 6-fold-coordinated Sn and Ti surface atoms. This polarization suggested the formation of an additional bond between the 6-fold-coordinated Ti-6c and bridging O atoms that had to be broken upon H2O adsorption. As a result, the H2O adsorption energy initially decreased, with increasing surface Ti content reaching a minimum at 25% Ti for 1/12 ML. This behavior was even more accentuated at high H2O coverage (1 ML) with the adsorption energy decreasing rapidly from 145.2 to 101.6 kJ/mol with the surface Ti content increasing from 0 to 33%. A global minimum of binding energies at both low and high coverage was found between 25 and 33% surface Ti content, which may explain the minimal cross-sensitivity to humidity previously reported for Sn1-xTixO2 gas sensors. Above 12.5% surface Ti content, the binding energy decreased with increasing coverage, suggesting that the partial desorption of H2O is facilitated at a high fractional coverage.

DOI: https://doi.org/10.1021/la204124p

First Principles Analysis of H_2O Adsorption on the (110) Surfaces of SnO_2, TiO_2 and their Solid Solutions

Konstanze R. Hahn,[1] Antonio Tricoli,[2] Gianluca Santarossa,[2,3] Angelo Vargas,[3] Alfons Baiker[3*]

[1]Institute of Physical Chemistry, University of Zurich, 8057 Zurich, Switzerland

[2]Department of Mechanical and Process Engineering, ETH Zurich, 8092 Zurich, Switzerland

[3]Department of Chemistry and Applied Bioscience, ETH Zurich, 8093 Zurich, Switzerland

October 2011

*corresponding author: baiker@chem.ethz.ch, Tel: +41 (0)44 632 31 53; Fax: +41 (0)44 632 11 63

ABSTRACT

Associative and dissociative H_2O adsorption on $SnO_2(110)$, $TiO_2(110)$ and Ti-enriched $Sn_{1-x}Ti_xO_2(110)$ surfaces have been investigated at low (1/12 monolayer (ML)) and high coverage (1 ML) by density functional theory calculations using the Gaussian and plane waves formalism. The use of a large supercell allowed the simulation at low symmetry levels. On $SnO_2(110)$ dissociative adsorption was favored at all coverages accompanied by stable associative H_2O configurations. Increasing the coverage from 1/12 to 1 ML stabilized the (associatively or dissociatively) adsorbed H_2O on $SnO_2(110)$ due to the formation of intermolecular H-bonds. In contrast, on $TiO_2(110)$, adsorption of isolated H_2O groups (1/12ML) was more stable than at high coverage and favored adsorption changed from dissociative to associative with increasing coverage.

For dissociative H_2O adsorption on Ti-enriched $Sn_{1-x}Ti_xO_2(110)$ surfaces with Ti atoms preferably located on six-fold coordinated surface sites, analysis of the Wannier centers showed a polarization of electrons surrounding bridging O atoms that were bound simultaneously to six-fold coordinated Sn and Ti surface atoms. This polarization suggested the formation of an additional bond between the six-fold coordinated Ti_{6c} and bridging O atoms that had to be broken upon H_2O adsorption. As a result, the H_2O adsorption energy initially decreased with increasing surface Ti-content reaching a minimum at 25 % Ti for 1/12 ML. This behavior was even more accentuated at high H_2O coverage (1ML) with the adsorption energy decreasing rapidly from 145.2 to 101.6 kJ/mol with Ti content increasing from 0 to 33 %. A global minimum of binding energies at both low and high coverage was found between 25 and 33 % surface Ti-content which may explain the minimal cross-sensitivity to humidity previously reported for $Sn_{1-x}Ti_xO_2$ gas sensors. Above 12.5 % surface Ti-content, the binding energy decreased with increasing coverage suggesting that partial desorption of H_2O is facilitated at high fractional coverage.

INTRODUCTION

The semiconducting nature of many metal oxides makes them interesting materials for numerous industrial and economical important applications. Wide band gap semiconducting metal oxides such as SnO_2 and TiO_2 are used, for example, in solar cells[1,2], photocatalysis[3,4] and as chemoresistive portable gas sensors[5]. Since the pioneering work of Fujishima and Honda[3] in 1972 on photoinduced decomposition of H_2O on TiO_2, intensive research has been done to optimize the photocatalytic behavior of TiO_2 for hydrogen production from H_2O or hydrocarbons and for degradation of organic pollutants.[6,7] The main advantages of TiO_2-based materials in this area are their high stability, low costs and high photoactivity.[8,9] Considerable improvement of TiO_2 was achieved by substitutional or interstitial doping with anionic species, in particular nitrogen.[4,10] Doping with cationic metal atoms such as Pt[11] and Sn[12,13] has also shown to improve the photocatalytic behavior.

The performance of TiO_2-based photocatalysts used in gas-solid phase reactions varies significantly with the relative humidity.[14-16] At low H_2O content, degradation of pollutants is enhanced by an increased number of hydroxyl groups on the surface.[14] However, for higher water content the H_2O species are competing with the actual reactants,[14,15] reducing the reaction rates as it has been shown for trichloroethylene[15] and *m*-xylene[17]. Furthermore, H_2O species adsorbed on the TiO_2 surface decrease the upward band bending. This facilitates the recombination of electron and holes and reduces the photocatalytic activity.[9,16] Thus it is an important task to control the water adsorption properties on TiO_2-based catalysts in order to optimize their photocatalytic activity.

Another interesting field for semiconducting metal oxides is their use as chemoresistive gas sensors.[18] Their ability to change conductivity when gaseous molecules are reacting with the surface makes them particularly applicable for such devices.[19,20] Solid state gas sensors made of metal oxide nanoparticles are currently utilized for process safety control, environmental monitoring and homeland security.[21,22] They have been applied to human breath analysis to estimate the blood alcohol content of drunk drivers[23] and more recently for the detection and monitoring of breath markers for several diseases such as lung cancer[24] or diabetes.[25] Tin oxide (SnO_2) is the most widely used metal oxide for chemoresistive gas sensors.[26] Its sensitivity and selectivity depend also on the exposed facets of the rutile crystal structure.[27] Han et al.[28] synthesized SnO_2 particles with different morphology and found that octahedral particles with

exposed high-energy (221) facets show highest gas-sensing performance towards ethanol. However, the gas sensing performances reported in this article are rather poor compared to those found in other studies with exposed low-index SnO_2 facets such as (110), (101) and (100)[29]. Furthermore, such high-index (221) facets have a higher surface energy[28] and thus are more difficult to produce than spontaneously growing low-index facets[30].

High sensitivity and selectivity is in particular important for chemoresistive gas sensors used in non-invasive medical diagnostics (breath analysis) since the breath consists of more than 1000 volatile compounds and has a high relative humidity (r.h.).[31] This is particularly problematic as water vapor increases the electrical conductivity of the metal oxide upon reaction with its surface and thus results in an unreliable sensor response.[32,33] High cross-sensitivity to humidity is a major drawback of SnO_2, one of the most studied and widely used gas sensing metal oxides, sensitive to several relevant analytes such as CO, NO_x, H_2 and ethanol.[26] In fact, the reaction between water vapor and the SnO_2 surface leads to remarkable changes (up to 85%) in its sensor response.[32,33] Even for more selective sensing oxides such as WO_3, water vapor is a common problem[34] that limits its applicability to non-invasive medical diagnostics by breath analysis.

The understanding of the cross-sensitivity mechanism of gas sensing metal oxides to humidity is still in progress. As a result, there is a necessity for further research on the H_2O adsorption on wide band gap semiconducting metal oxides that overlaps with the interest to optimize such materials for photocatalysis. For adsorption of H_2O on SnO_2 and the resulting increase in electrical conductivity, three main paths have been proposed.[33] In the first mechanism, it is suggested that H_2O dissociates in an H atom and OH group that react further with the metal oxide surface. The OH group (terminal OH) binds to a surface metal atom, whereas the H atom binds to a rooted O atom resulting in a rooted OH group. The latter is then donating an electron to the conduction band[35] according to:

$$H_2O_{gas} + Sn^* + O^* \longrightarrow (Sn^{\delta+} - OH^{\delta-}) + (OH)^+ + e^- \qquad (1)$$

The asterisk indicates the active sites of the metal oxide surface, whereas ($Sn^{\delta+}$ - $OH^{\delta-}$) is referred to an isolated (terminal) hydroxyl group and $(OH)^+$ to a rooted OH group. Since the rooted O is normally in the (2-) state it can become ionized and function as an electron donor.

The second mechanism considers the formation of oxygen vacancies. In this mechanism, the rooted OH group reacts further and binds to a neighboring Sn atom producing an oxygen vacancy. This vacancy donates by ionization two electrons to the conduction band of the

semiconductor.[35] The third mechanism is described as an indirect process where pre-adsorbed species are changing the electron affinity of the surface.[36,37] This could be for instance the reaction of the adsorbed hydroxyl group or the hydrogen atom bond to rooted O which are acting as active sites on the surface and possibly react with acid or basic groups.[36,37]

Recently, it has been shown that altering the SnO_2 structure by introduction of impurities results in a drastic stabilization of the sensor response in the presence of varying water vapor content.[5] Doping of SnO_2 nanoparticles with low Ti-content (4.6 at%) decreased the cross-sensitivity to r.h. remarkably while maintaining high sensitivity towards the tested analyte (ethanol). At the optimal doping content, a residual cross-sensitivity to r.h. of ca. 15% was measurable increasing the r.h. from 0 (dry air) to 20%. Further increase of the r.h. did not have any effect on the sensor signal. This approach was particularly convenient as both metal oxides (SnO_2 and TiO_2) share a rutile crystal phase and their co-synthesis at high temperature (>2000K) promoted the formation of a substitutional solid solution without any segregation up to 80 at% of Ti.

The two metal oxides, SnO_2 and TiO_2, have noticeable differences in electronic and adsorption properties due to the fact that Ti is a transition metal and Sn is a group IV element. In terms of sensitivity and conductivity, TiO_2 is inferior to SnO_2.[18] Nevertheless, it has a higher thermodynamic stability and less cross-sensitivity to humidity than SnO_2.[26] Experimentally studied $Sn_{1-x}Ti_xO_2$ nanoparticles[5] combined the advantages of both metal oxides but the fundamental understanding of the H_2O interaction with their surface is still sought for.

In this regard, theoretical investigation of the $Sn_{1-x}Ti_xO_2$ system represents a unique opportunity to achieve a better understanding of the mechanisms controlling the adsorption properties of H_2O on wide band gap semiconducting metal oxides for application in gas sensing and photocatalysis. Among computational methods, density functional theory (DFT) is a quantum mechanical method that is widely used to describe catalytic processes mainly on crystal metal surfaces.[38-40] Furthermore, it has been proven to be an appropriate method for the calculation of metal oxide surfaces.[41-45] In fact, DFT has been applied to evaluate the stability of stoichiometric pure SnO_2 and TiO_2 surfaces showing that for both crystals the (110) surface is the most favored. Moreover, the $Sn_{1-x}Ti_xO_2$ bulk system has been studied by DFT[46] confirming the experimentally measured variation from Vegard's law for the rutile lattice parameters.[5,47] Adsorption properties of H_2O on the pure SnO_2 and TiO_2(110) surfaces have been studied extensively by DFT. It has been shown that H_2O tends to dissociate spontaneously on the

SnO_2(110) surface at high coverages, indicating that dissociative adsorption is favored over associative one.[48,49] In contrast for TiO_2, associative adsorption is favored over dissociative adsorption at full coverage[50] while dissociative adsorption becomes favorable at low coverage.[51]

In this study, we have used DFT calculations with Gaussian plane wave (GPW) basis sets[52,53] to investigate the H_2O adsorption properties on $Sn_{1-x}Ti_xO_2$ solid solutions. The GPW approach allows the simulation of large systems with good computational efficiency. First, the binding energies and geometrical properties for dissociative and associative H_2O adsorption were computed on the pure SnO_2 and TiO_2 surfaces at high and low H_2O coverages to verify the consistence with previous works. The dissociative adsorption energy was then evaluated for $Sn_{1-x}Ti_xO_2$ solid solutions as a function of the Ti-content providing an explanation for the minimal cross-sensitivity to humidity observed for gas sensors made of such solid solutions.

METHODS

Computational Details. The simulations performed in this investigation were based on DFT as implemented in the CP2K program package, a suite of programs aimed at performing efficient electronic structure calculations and molecular dynamics at different levels of theory.[54] Rutile type metal oxides can be simulated with good agreement to experimental results using exchange-correlation potentials with general gradient approximation (GGA).[41] The electronic structure calculations employ the Gaussian and plane wave (GPW) formalism.[52,53] Interaction of valence electrons with frozen atomic cores was described using norm conserving, dual-space type pseudopotentials.[55] For Sn and Ti metal atoms, 4 and 12 electrons were explicitly considered, respectively, in the valence shell. A double-zeta valence plus polarization (DZVP) basis set, optimized according to the Mol-Opt method[56] has been adopted for the metal atoms and hydrogen and a triple-zeta valence plus polarization for oxygen. For auxiliary PW expansion of the charge density, the energy cutoff has been set at 400 Ry. Exchange-correlation potentials were modeled using the Perdew-Burke-Ernzerhof (PBE) functional.[57]

The size of the simulation domain is a critical parameter in real space calculations. It defines the accuracy of the density, the accuracy of the physical system and the computational time frame needed. The optimal compromise between physical accuracy and resource allocation for the present investigation was found to be a supercell of 720 atoms. The rutile primitive cell has been repeated 3 and 4 times along the x and y directions, respectively. Along the z-direction, the cell

has been repeated 10 times, in order to form a slab of ten metal atom layers. All simulations were performed with periodic boundary conditions. Determination of the optimal lattice parameters *a*, *c* and *u* has been carried out by self-consistent wave function calculations for different lattice values until the convergence in the total energy was lower than 10^{-3} eV per metal atom of the super cell. The cell parameters for $Sn_{1-x}Ti_xO_2$ solid solutions were optimized with Ti atoms distributed in the bulk. The optimized parameters can be found elsewhere.[58] The simulations with Ti-surface distribution were performed using the parameters optimized for bulk calculations. To simulate the surface, 10 Å of vacuum were added along the z-direction in order to avoid any interaction of the cluster with its periodic image. Three metal atom layers on the top and the bottom of the slab were allowed to relax in all dimensions while four layers were fixed to simulate the bulk corresponding to the simulation domain used previously[58] investigating the stability of $Sn_{1-x}Ti_xO_2$(110) surfaces.

The adsorption of H_2O was simulated on one of the exposed surfaces of the slab. It is supposed that placing adsorbates on both sides gives more accurate results since possible dipoles are eliminated.[59] However, calculations with adsorbates on both sides showed a difference in binding energy of less than 3.5 kJ/mol. Thus, it was concluded that precise values of the binding energy are yielded also when simulating adsorption only on one surface. The H_2O binding energies (E_B) were calculated according to:

$$E_B = \frac{E_{slab+nH_2O} - (E_{slab} + n \cdot E_{H_2O,g})}{n} \qquad (2)$$

where *n* gives the number of adsorbed species on the described surface and $E_{slab+nH2O}$ denotes the energy of the surface slab plus *n* adsorbates. The energy of an isolated H_2O molecule ($E_{H2O,g}$) was calculated in a periodically repeated cell of 20 Å. Here, the surface plane consisted of 12 unit cells meaning that full H_2O coverage (1 ML) corresponds to 12 adsorbed H_2O groups.

Surface metal atoms (Fig. 1) bound to five or six neighboring O atoms were named as Me_{5c} or Me_{6c}, respectively. Rooted O atoms that are located in the surface layer were denoted as O_r, whereas bridging O atoms are denoted as O_{br} (Fig. 1). The O atoms where H_2O was associatively adsorbed were denoted as O_{H2O}.

RESULTS AND DISCUSSION

On pure SnO_2 and TiO_2, associative and dissociative chemisorption of water at different coverages was simulated. For associative adsorption, the bonds of the water molecule were preserved and the H_2O molecule was placed perpendicular to the surface with the oxygen atom (O_{H2O}) bound to a fivefold coordinated metal atom site.[44,50] In contrast, for dissociative adsorption, one H atom was separated from the H_2O molecule (Fig. 1). The OH group was bound to a five-fold coordinated (5c) metal atom (Me_{5c}), resulting in a terminal OH group (OH_{term}), and the separated H atom was bound to a bridging O (O_{br}), resulting in a rooted OH group (OH_{root}). This mechanism was proposed previously for dissociative H_2O adsorption on rutile (110) surfaces.[48,50,60] For dissociative H_2O adsorption, the interaction between surface OH groups plays an important role. In the following, the distance between the H atom of an OH_{root} group and the O atom of an OH_{term} group is denoted as d_{root} and the distance between H and O atom of two adjacent terminal groups as d_{term} (Fig. 1a).

Adsorption on SnO_2(110)

Isolated Adsorption (1/12 ML). Associative adsorption of an isolated H_2O molecule (1/12 ML) was found to be stable in a perpendicular configuration (Fig. 2a,b). The distance between Sn_{5c} and O_{H2O} was 2.28 Å. Additionally to the perpendicular configuration, the H_2O molecule was initially placed parallel to the surface (not shown). In this case, however, the H_2O molecule dissociated spontaneously. In the dissociated configuration, the Sn_{5c}-OH_{term} (Fig.1b) bond length was remarkably smaller (2.02 Å) indicating a stronger bond. This Sn_{5c}-OH_{term} bond length was equal to that between Sn_{6c} and O_{br} of the clean SnO_2(110) slab[58] suggesting similar characteristics to the Sn-O bonds.

The distance between H atoms of an associatively adsorbed H_2O molecule and O_{br} was 2.86 Å (Fig. 2a). For dissociative adsorption, smaller intermolecular distances were found: The H atom of the OH_{root} group and the O atom of the OH_{term} had a distance (d_{root}) of 2.36 Å (Fig. 2d). This indicated the presence of additional attractive interactions for dissociative adsorption. It was further observed that the H atom of the OH_{term} group pointed towards the nearest O_{br} atom (opposite of the OH_{root} group, 3.11 Å, Fig. 2d). Thus, approaching of the two OH groups as it was observed at higher coverages (1.94 Å[44]) was prevented.

The binding energy of associatively adsorbed H_2O was 98.8 kJ/mol, whereas for dissociative adsorption it was significantly larger amounting to 135.2 kJ/mol. Based on these results, it is

concluded that at low coverage H_2O tends to dissociate on the $SnO_2(110)$ surface. The stabilization of dissociated H_2O can be explained by attractive interactions between the OH groups and a stronger bond between Sn_{5c} and the O of the OH_{term} group.

High coverage adsorption (1 ML)

Structural properties. For associatively adsorbed H_2O, the initial configuration was perpendicular to the surface as set for the isolated H_2O adsorption (1/12 ML). However, at this high coverage the H_2O molecules bent towards the surface resulting in a parallel associative adsorption configuration (Fig. 3a). This is in contrast to what was observed (see discussion above) for isolated H_2O molecules which spontaneously dissociated when initially positioned in a parallel configuration. As a result, at high coverage, the distance between an H atom and an O_{br} atom was reduced to 1.42-1.88 Å (Fig. 3a) due to this bending of the molecules towards the surface. It is suggested that these H-bonds are stabilizing the H_2O on the surface at high coverage. The intermolecular distance between two H_2O molecules was 2.49 Å (Fig. 3a) indicating additional attractive interactions that are not present for isolated H_2O. The latter presumably affected the electron density around the H pointing to the O_{br} atom hindering the dissociation of an H atom as it was observed for isolated H_2O. The distance between the O_{H2O} atom and the Sn_{5c} atom (Sn_{5c}-O_{H2O}) was larger for 1 ML associative adsorption (2.39 Å) than at low coverage (2.28 Å) indicating weaker bonds.

For dissociative adsorption, the d_{root} distance (Fig. 1a) was remarkably smaller at high coverage (1.80 Å, Fig. 4a) than at low coverage (2.36 Å) indicating enhanced H-bonds. At high coverage, the H atom of OH_{term} groups was attracted by the O atom of a neighboring OH_{term} group. In contrast, at low coverage, the H atom of the OH_{term} group was attracted by an adjacent O_{br} (3.11 Å, Fig. 2d) atom leading to a larger d_{root} distance.

Moreover, the neighboring OH_{term} groups showed additional attractive interactions between the H and O atom of two adjacent groups that was not possible for isolated H_2O adsorption. The distance between these H and O atoms (d_{term}) was 2.49 Å. The bond length between Sn_{5c} atoms and an OH_{term} group (Sn_{5c}-OH_{term}, Fig. 1b) was similar for both high (2.06 Å) and low (2.02 Å) coverage indicating same bond characteristics for both coverages. These values were close to the bond length between Sn_{6c} and O_{br} (2.02 Å) of the clean $SnO_2(110)$ surface.[58]

Additional to pure associative and dissociative configurations, a stable state was found in a mixed configuration where half of the molecules dissociated and the other half was adsorbed

associatively (Fig. 3b). This configuration resembles the one found for partial H_2O dissociation on Ru(0001) where a hexagonal pattern was formed.[61] On SnO_2, the Sn_{5c}-O_{H2O} bond length was with 2.25 Å similar to that (2.28 Å) for isolated H_2O adsorption suggesting similar bond characteristics. The bond length between Sn_{5c} and the dissociated OH_{term} groups (2.09 Å) was close to that for pure dissociative adsorption at high (2.06 Å) coverage and isolated H_2O (2.02 Å). The complete geometrical properties are reported in Figure 3b.

Stability. Pure associative adsorption of H_2O at 1 ML had a binding energy of 112 kJ/mol (Fig, 3a, Table 1). The same binding energy (113 kJ/mol) was computed in a previous study using a smaller unit cell with the PBE exchange-correlation functional.[49] However, in the latter, artificial constraints were introduced for the relaxation to prevent spontaneous dissociation of the H_2O molecules. Figure 3a shows that the H_2O molecules bound to the left and the middle column of Sn_{5c} atoms pointed towards the O_{br} atom on their left side, whereas the H_2O molecules of the last column pointed towards the O_{br} atom on their right side resulting in an asymmetric configuration. Previous DFT studies applying the planewaves approach showed that molecular H_2O on rutile (110) SnO_2 is neither stable for a complete nor half a monolayer coverage of H_2O.[44,48,49,62] There, water molecules placed initially above a fivefold coordinated Sn atom dissociated spontaneously into OH and H. However, the unit cells used in those studies had a surface about three times smaller than that used here. The use of smaller cells restricts the possible configurations of adsorbates and their periodic repetition leads to more symmetric arrangements of adsorbed species. To understand the destabilizing effect of higher orientation symmetry (all H_2O molecules pointing into the same direction), the water molecules of the third column (Fig. 3a) were artificially placed so that they pointed all into the same direction. This led to dissociation of half the H_2O molecules (Fig. 3b) resulting in a mixed associative and dissociative adsorption state with a binding energy of 137.8 kJ/mol (Table 1). An associative configuration was found in previous studies using a smaller unit cell[48,49] but required the utilization of the hybrid functional B3LYP.[44] This was attributed to the larger H-bond length in hybrid DFT calculations such as B3LYP (than in plain ones) that inhibited the formation of covalent bonds and thus H_2O dissociation.[44] However, the results presented here demonstrate that spontaneous dissociation of H_2O on SnO_2(110) is not only affected by the functional used but also by constraints resulting from the use of a small unit cell with periodic boundary conditions which lead to unreasonably high symmetry configurations.[44,49] Here, for the first time, a stable state for associative adsorption configuration was established in a more asymmetric configuration

using a standard exchange-correlation potential (PBE). Such associative adsorption is consistent with experiments showing the presence H_2O molecules on the SnO_2(110) surface.[60] This suggests that restrictions of the system size have to be considered as potential sources of errors in DFT calculations.

Pure dissociative adsorption at 1 ML H_2O resulted in a binding energy of 145.2 kJ/mol. Again, this was in very good agreement with previous results[49] reporting a value of 141 kJ/mol. It was significantly more stable than associative adsorption (112 kJ/mol) (Table 1), similarly to that observed for isolated H_2O adsorption. For all coverages simulated in this study, on SnO_2, the binding energies of dissociative H_2O (135.2-145.2 kJ/mol) adsorption were higher than that of associative H_2O adsorption (98.8-112.0 kJ/mol) demonstrating that H_2O molecules preferably adsorb dissociatively on SnO_2(110) independent of the coverage.

The analysis of the geometry suggested the presence of intermolecular H-bonds at high H_2O coverage for both associative and dissociative adsorption. These H-bonds stabilized the adsorbates and resulted in higher binding energies at high coverage. In contrast, H-bonding was previously considered to play only a marginal role for H_2O adsorption on SnO_2.[50] Furthermore, the higher binding energies at high coverage indicate that on SnO_2 adsorption of H_2O is enhanced with increasing water content. For the use of SnO_2 as a gas sensor, this means that the higher the relative humidity the more H_2O is adsorbed. Consequently, the conductivity and response of SnO_2 gas sensors depend on the relative humidity also at relatively high humidity concentration.

Adsorption on TiO_2(110)

Isolated Adsorption (1/12 ML). On TiO_2, in contrast to SnO_2, associatively adsorbed H_2O was stable both in configurations perpendicular (not shown, cf. Fig. 2a,b) and parallel (Fig. 5a,b) to the surface. The bond length between Ti_{5c} and O_{H2O} was similar for both configurations (2.25 Å and 2.26 Å) and close to that on SnO_2 (2.28 Å). Despite the smaller lattice parameters of TiO_2 (a = 4.64 Å and c = 2.98 Å)[58], the perpendicular H-O_{br} distance (2.87 Å) was similar to that on SnO_2 (2.86 Å). This suggests that the H-O interaction is hardly affected by the dimension of the lattice or by the metal atom type (Sn or Ti).

For dissociatively adsorbed H_2O, the Ti_{5c}-OH_{term} distance (1.82 Å, Fig. 5c) was remarkably smaller than for associative adsorption and, as observed for SnO_2, close to the Ti_{6c}-O_{br} distance of the clean TiO_2(110) surface (1.83 Å).[58] For dissociation of the H_2O molecule, d_{root} (Fig. 5c) of 2.30 Å was found.

The perpendicular configuration (92.0 kJ/mol) of an H_2O molecule was slightly more stable than the parallel one (89.5 kJ/mol, Table 2). Dissociation was, similar to SnO_2, favored over both types of associative configurations with a binding energy of 99.4 kJ/mol (Table 2).

High Coverage Adsorption (1 ML)

Structural Properties. For 1 ML associatively adsorbed H_2O, the distance between the H atom and O_{br} was with 2.11 Å (Fig. 3c) remarkably larger than that on SnO_2 (1.42-1.88 Å, Fig. 3a) regardless of the smaller lattice parameters of TiO_2. This suggests, that H-bonds between adsorbates and surface are less pronounced on TiO_2. The Ti_{5c}-O_{H2O} distance was larger at high coverage (2.40 Å) than for both perpendicular (2.25 Å) and parallel (2.25 Å, Fig. 5a) configuration at low coverage as observed for SnO_2. This indicates that at high coverage, the Ti-O bond is weaker. The distance between H and O_{H2O} was smaller (2.15 Å, Fig. 3c) on TiO_2 than on SnO_2 (2.49 Å, Fig. 3a) in agreement with the smaller lattice parameters of TiO_2.

For dissociative adsorption, d_{root} at high coverage (2.37 Å, Fig. 5d) was larger than for isolated adsorption (2.30 Å, Fig. 5d), indicating repulsive intermolecular interactions. Thus, on TiO_2, no stabilization but rather marginal destabilization was established at high coverage for dissociative H_2O adsorption. In agreement with the different lattice parameters, d_{term} was smaller on TiO_2 (2.16 Å, Fig. 4d) than on SnO_2 (2.49 Å, Fig. 4a). The Ti_{5c}-OH_{term} distance at high coverage (1.87 Å, Table 4) was similar to that (1.82 Å) for isolated adsorption and close to the Ti_{6c}-O_{br} distance of the clean TiO_2 (110) surface (1.83 Å).[58]

Stability. At 1 ML, associative H_2O adsorption on TiO_2 (Fig. 3c) resulted in a binding energy of 78.7 kJ/mol (Table 2). Similar values (83-95.5 kJ/mol) were reported previously for associative H_2O adsorption on TiO_2 at high coverage.[49,50] Dissociatively adsorbed H_2O (Fig. 4d) was found to be less stable with a binding energy of 60.3 kJ/mol. This is again in reasonable agreement with previous studies (66-87.9 kJ/mol).[49,50,63] Partially dissociated H_2O (75.4 kJ/mol, not shown) was slightly less stable than pure associative and dissociative adsorption. This is in contrast to SnO_2 where partial dissociation of H_2O (Fig. 3b) was found to be favored over pure associative adsorption and is in agreement with the observed stabilization effect of H-bonds.

For both associative and dissociative adsorption, the binding energy at high coverage (78.7 kJ/mol and 60.3 kJ/mol, respectively) was lower than at low coverage (92.0 kJ/mol and 99.4 kJ/mol, respectively) suggesting the presence of repulsive interactions between adsorbed species. This is in contrast to SnO_2, where H_2O was more stable at high coverage. There the

stabilizing effect was attributed to the formation of H-bonds between H and O_{br} (1.42-1.88 Å, Fig. 3a) for associative adsorption and between OH_{term} and OH_{root} groups (d_{root}(1 ML) =1.80 Å) for dissociative adsorption. Both distances (2.11 and 2.37 Å, respectively) were larger on TiO_2, indicating a lack of intermolecular attraction. As a result, on TiO_2, the binding energy decreased with increasing H_2O coverage. In other words, on TiO_2, H_2O adsorption is facilitated at low H_2O content in contrast to SnO_2. This implies that the saturation coverage is dependent on the temperature and can be reached already at a low relative humidity at a certain temperature. Furthermore, a larger spread between high and low coverage binding energy was observed compared to SnO_2.

On the TiO_2(110) surface, the binding energies showed that, for isolated adsorption, the H_2O molecules preferred to dissociate whereas associative adsorption was favored at high coverage. Thus, the preferred adsorption mechanism changed with the coverage. There has been discrepancy about the favored adsorption mechanism on TiO_2 (110) in the literature previously.[43,50,51,63,64] Some DFT studies[43,51] using the plane-waves formalism and the revised PBE exchange-correlation functional revealed that the dissociative mechanisms is favored at low coverages ($\theta \leq 0.5$ ML), whereas others[63] using the PW91 functional stated that associative adsorption is favored for coverage ≤1 ML. Experimental studies using TPD, however, determined a tail of the desorption peak extending to higher temperatures (100 °C) which was attributed to hydroxyl groups.[65] This confirmed the presence of dissociated H_2O at low coverages. On the other hand, at high H_2O doses (high coverage), molecular species were detected[65,66] which supports the higher binding energy of associative adsorption at 1 ML found in this study. Furthermore, TPD analysis[65,66] at lower H_2O doses showed a shift of the H_2O desorption peak to higher temperatures. This indicates a higher desorption energy at lower H_2O coverage which can be attributed to less dipole-dipole repulsion between adsorbed species in agreement with our findings.

Adsorption on $Sn_{1-x}Ti_xO_2$(110)

On $Sn_{1-x}Ti_xO_2$ solid solutions dissociative H_2O adsorption was investigated for isolated species (1/12 ML) and full (1 ML) coverage. It has been shown previously that Ti is preferably distributed in the surface layer of $Sn_{1-x}Ti_xO_2$ solid solutions,[58] more specific on six-fold coordinated (6c) surface sites.[58,67] Therefore, here, H_2O adsorption mechanisms were investigated on $Sn_{1-x}Ti_xO_2$ (110) surfaces with Ti atoms located exclusively on 6c-sites up to a surface Ti-

content of 50 % where all 6c sites were occupied by Ti. For higher surface Ti-content, up to 100 %, Ti atoms were distributed additionally on 5c sites. The binding energy shown in Figure 7 represents an average value for the different binding sites at a specific surface Ti-content.

Isolated Adsorption (1/12 ML)

Structural Properties. Adsorption of isolated H_2O groups was investigated on all possible surface sites at each Ti-content. Accordingly, Table 3 summarizes the results averaged on all possible sites. The Me_{5c}-OH_{term} bond length hardly changed compared to that on pure SnO_2 (2.02 Å) and TiO_2 (1.82 Å). In contrast, the average d_{root} distance increased from 2.36 to 2.50 Å with increasing surface Ti-content from 0 to 100 % and was always larger than that observed for pure TiO_2 (2.30 Å). The increase of d_{root} indicated reduced interactions and could possibly lead to weaker bond strength. The large scatter at 67% surface Ti-content resulted from a high level of irregular surface restructuring.

Electronic structure. For the representation of isolated H_2O adsorption, only a section of the surface is shown (Fig. 6) since surface configurations were relevant only in the vicinity of the adsorbate. To describe the adsorption properties, the centers of the Wannier functions were determined before (Fig. 6, left side) and after (Fig. 6, right side) H_2O adsorption. Green spheres in Figure 6 visualize the position of the Wannier centers around O_{br} atoms.

On pure SnO_2(110) (Fig. 6a), four Wannier centers were close to O_{br}, two of which pointed towards the adjacent Sn_{6c} atoms (in [001] direction). The other two were oriented out of the surface in [110] direction indicating two free electron pairs. Upon dissociative H_2O adsorption, one of these free electron pairs was transformed into a bond with the H atom (Fig. 6a, right side). When some Sn_{6c} atoms were substituted with Ti atoms some O_{br} were bound to both metal atom types (Fig. 6b) resulting in a reorientation of the Wannier centers. In this situation, one center pointed to the Sn_{6c} atom while two centers pointed to the Ti_{6c} atom suggesting the formation of an additional bond between O_{br} and Ti_{6c}. In other words, the O_{br} atom formed a total of three bonds to the adjacent metal atoms and had one free electron pair. For the O_{br}-H bond formation, here, one of the O_{br}-Ti_{6c} bonds (Fig. 6b, right side) had to be broken. The required energy for this step was reflected in a lower binding energy of H_2O (Fig. 7) on such surfaces. Regarding the reverse step this means that less energy, e.g. a lower temperature, is needed to remove H_2O from the $Sn_{1-x}Ti_xO_2$ surfaces.

At surface Ti-contents >25 %, two or more Ti_{6c} atoms can be adjacent to each other (Fig. 6c).

In these cases, the neighboring Ti_{6c} equally polarized the electrons (Wannier centers) of the enclosed O_{br} atom resulting in a single O_{br}-Ti_{6c} bond each (Fig. 6c) and a total of two bonds of the O_{br} atom. A correlation was found between the H_2O binding energy and the bonds formed by O_{br}. For this, the fraction of O_{br} atoms forming a total of three bonds to adjacent Me_{6c} atoms was analyzed as a function of the surface Ti-content (Fig. 7, circles). It was maximal at 25 % surface Ti-content. The converse behavior was observed for the average binding energy. The average binding energy of all possible adsorption sites on the surface decreased (Fig. 7, diamonds) since the number of O_{br} with three bonds increased with the surface Ti-content up to 25 % (Fig. 7, circles). However, further increase of the surface Ti-content decreased the number of O_{br} with three bonds and thus the average binding energy increased.

At surface Ti-contents between 25 and 50 % (Fig. 6c) an additional effect was observed leading to an increase of the binding energy. When the H atom was bound to an O_{br} site between Sn_{5c} and Ti_{6c}, i. e. with three bonds, one Ti-O_{br} bond was broken. However, this change in the electronic structure led to a shift of all connected Ti_{6c} atoms in [001] direction closer to the O_{br} atoms (Fig. 6c, right side). This induced the formation of additional Ti_{6c}-O_{br} which was reflected in an increased binding energy (by ca. 10 kJ/mol) on such sites.

Higher surface Ti-contents (50-100 %) increased the surface reconstruction and formation of additional Ti_{6c}-O_{br} and Ti_{5c}-O_r bonds on the surface. Here, the H_2O adsorption led to enhanced rearrangements of the geometrical and electronic structure dependent on the local environment of the active site. Decrease of the symmetry of the surface with increasing surface Ti-content was reflected in an increased range of binding energies for different surface sites (Fig. 9). This made it difficult to draw a general conclusion for surface Ti-contents >50 %. However, it is assumed that, in the case of low coverage, H_2O species adsorb on the energetically most favorable site. Thus, the highest binding energy for each Ti-content is relevant for the determination of the adsorption characteristics. As a result, a global minimum of the H_2O binding energy for isolated adsorption (1/12 ML) was found at a surface Ti-content of 25 % suggesting that, for this Ti-content, the temperature needed to desorb small amounts of H_2O species from the surface is lowest.

High Coverage Adsorption (1 ML)

Structural Properties. At high coverage, d_{root} increased drastically from 1.86 to 2.49 Å when increasing the surface Ti-content from 0 to 33 %. This demonstrated a loss of H-bonds between

adjacent OH groups that were observed on pure SnO_2. Further increase of the Ti-content hardly had any effect (2.41±0.1 Å) on d_{root}. It was close to that on pure TiO_2 (2.37 Å) indicating that d_{root} was rather determined by the surface composition than by the lattice parameters. In contrast, only marginal changes were observed for the d_{term} and the Sn_{5c}-OH and Ti_{5c}-OH bond length. A slight decrease of d_{term} from 2.49 to 2.41 Å (Table 4) was observed with increasing surface Ti-content, consistent with the decreasing lattice parameters.[58] The influence of the lattice parameters was as well reflected in the drop (0.25 Å) of d_{term} between 100% surface Ti-content, corresponding to 20% total Ti-content (2.41 Å), and pure TiO_2 (2.16 Å). When Ti atoms were introduced in the surface layer (17-67%), Sn_{5c}-OH_{term} decreased from 2.06 Å for pure SnO_2 to 2.03 Å (Table 4). The Ti_{5c}-OH bond length, on the other hand, was equivalent to that on pure TiO_2 (1.87 Å) indicating that the characteristic of this bond is determined by the chemical nature of the Me_{5c} atom rather than the surrounding atoms.

Stability. The binding energy at high coverage (1 ML) decreased rapidly from 145.2 to 101.6 kJ/mol with increasing surface Ti-content from 0 to 33 %. Further increase of the surface Ti-content up to 100 % had only marginal effect (±3.4 kJ/mol) (Fig. 8, diamonds, Fig. 9, filled diamonds). The behavior of the binding energy correlated well with d_{root} (Fig. 8, circles): a decrease in the binding energy was related to an increase in the H-O distance. This verifies the stabilization of adsorbed species by intermolecular H-bonds which can be quantified by d_{root}. For 100 % surface Ti-content, the binding energy (101.8 kJ/mol) was still remarkably higher than that on pure TiO_2 (60.3 kJ/mol). This suggests that the underlying SnO_2 crystal contributes considerably to the adsorption properties.

In summary, a minimum of the adsorption binding energy of isolated dissociatively adsorbed H_2O was evidenced for a surface Ti-content of 25%. This minimum is attributed to the maximum number of O_{br} atoms with three bonds to neighboring Me_{6c} atoms which had to be broken upon H_2O adsorption. Furthermore, the high coverage binding energy dropped rapidly from 145.2 to 101.6 kJ/mol with increased surface Ti-content from 0 to 33 %. Higher surface Ti-contents had almost no effect on the high coverage binding energy of H_2O. This led to an overall minimum of all binding energies between 25 and 33 % surface Ti-content. A qualitatively similar minimum was found experimentally at a total (surface + bulk) Ti-content of 4.6 % for the cross-sensitivity to humidity of FSP-made $Sn_{1-x}Ti_xO_2$ nanoparticles. However, no explanation could be given yet for this behavior.[5] Assuming that all Ti atoms are distributed on the particle surface and the particles have an average size between 9 and 11 nm, the surface Ti-content of such particles is

approximately 24 to 29 % and thus in good agreement with the computed surface Ti-content for the minimum of the H_2O binding energy. This suggests that dissociative H_2O adsorption plays a key role in the cross-sensitivity mechanisms to humidity of SnO_2-based gas sensors. Furthermore, it supports the proposed homolytic dissociation of water on SnO_2 that leads to an increase in its conductivity.[32,33,35] It has been shown previously that Sn-doping of TiO_2 catalysts leads to enhanced photoactivity[13] which was partly attributed to the decrease of the band gap.[13,68] The results of the present study suggest additionally that the dependency of the catalytic activity on the relative humidity can be minimized for an optimal Sn:Ti ratio.

Moreover, the rapid decrease of the 1 ML binding energy caused adsorbed H_2O to be more stable at low coverage (Fig. 9, open diamonds) than at high coverage (Fig. 9, filled diamonds). Already at a surface Ti-content of 33 %, repulsive interactions between adsorbed species were more pronounced than attractive ones (H-bonds). The amount of adsorbed H_2O is not only dependent on the relative humidity but also on the process conditions such as temperature. This gives a possible explanation for the remaining minimal cross-sensitivity (15 %) of FSP-made $Sn_{1-x}Ti_xO_2$ nanoparticles that was shown experimentally.[5] In fact, there, the working temperature of the gas sensor (320 °C) was most probably high enough to overcome the binding energy at full coverage. However, due to the increased binding energy at low coverages, trace amounts of H_2O remained on the surface leading to a variation of the sensor signal measured in dry air and thus to a small cross-sensitivity residual.

Furthermore, the difference between H_2O binding energy at high and low coverage became larger with increasing surface Ti-content due to the drop of the binding energy at 1 ML and the rise of the one at 1/12 ML for surface Ti-contents >25 % (Fig. 9). Assuming a linear dependency of the binding energy on the coverage, it is suggested that controlling of the amount of adsorbed H_2O species by the temperature is facilitated when the difference between low and high coverage binding energy gets larger.

Finally it should be stressed that our theoretical study of H_2O adsorption on TiO_2, SnO_2 and $Sn_{1-x}Ti_xO_2$ surfaces and its impact on the cross-sensitivity of gas sensors only holds rigorously for equilibrated systems. However, it may also reflect the tendencies to be expected under dynamic conditions and therefore help in the interpretation of the relation between water adsorption and its impact on the cross-sensitivity.

CONCLUSIONS

The binding energy of dissociatively and associatively adsorbed H_2O was calculated on pure SnO_2(110) and TiO_2(110) at high coverage (1 ML) and for isolated species (1/12 ML). On pure SnO_2, a stable configuration was found for 1 ML associatively adsorbed H_2O using plain DFT calculations in agreement with experiments. This was possible by the simulation of a larger unit which reduced the level of symmetry. In agreement with previous calculations, dissociative adsorption is shown to be the favored mechanism for all coverages. Independent of the adsorption mechanism, the formation of H-bonds was observed on SnO_2, leading to a higher binding energy at high coverage compared to that at low coverage.

On TiO_2, the favored adsorption mechanism changed with coverage. Isolated H_2O groups tended to dissociate, while at high coverage, associative adsorption was favored. For both adsorption mechanisms, the binding energy at low coverage was higher than at high coverage. These finding are in agreement with TPD experiments which show a shift of H_2O desorption to higher temperatures at low doses.

On $Sn_{1-x}Ti_xO_2$(110) with homogeneous surface Ti distribution, the binding energies for dissociative adsorption were determined at high and low coverages. Analysis of the Wannier centers at low coverage suggested the formation of additional bonds between Ti_{6c} and bridging O_{br} atoms. These have to be broken upon H_2O adsorption resulting in a decrease of the binding energy up to a surface Ti-content of 25 %. At higher Ti-contents, less additional Ti_{6c}-O_{br} bond formation was observed due to the effect of neighboring Ti_{6c} atoms. This caused again an increase of the low coverage binding energy at Ti-contents >25 %.

The binding energy at high coverage on $Sn_{1-x}Ti_xO_2$(110) decreased rapidly with increasing surface Ti-content up to 33 %. This is attributed to the loss of H-bonds indicated by a larger distance between neighboring OH groups (d_{root}). Higher surface Ti-contents had hardly any effect on the binding energy. Already at 12.5 % surface Ti-content, H_2O adsorption at low coverage was more stable than at high coverage. In this case it is suggested that the amount of adsorbed H_2O can be controlled by process parameters such as temperature.

Considering both high and low coverage binding energies, a global minimum was found between 25 and 33 % surface Ti-content. This minimum in binding energy gives a possible explanation to the previously observed minimum in cross-sensitivity to humidity of $Sn_{1-x}Ti_xO_2$ nanoparticle-based gas sensors. Furthermore, it supports the proposed interaction mechanism between SnO_2 and H_2O vapor based on the homolytic dissociation of H_2O on Sn_{5c}

and O_{br} atoms.

The results of this study show that already small amounts of Ti on the $SnO_2(110)$ surface significantly change the H_2O adsorption behavior and that first-principles calculations can aid in designing mixed metal oxides with specific H_2O adsorption characteristics. Controlling the H_2O adsorption and reaction mechanism on the desired metal oxides can improve the performance of such materials both in the fields of gas sensors as well as photocatalysis.

ACKNOWLEDGMENT

This research was supported in part by the European Research Council and Swiss National Science Foundation. Computational time was provided by ETH and the Swiss National Supercomputing Center. We are grateful for inspiring discussions with M. Iannuzzi and J. Hutter.

REFERENCES

[1] Wager, J. F. *Science* **2003,** *300*, 1245-1246.

[2] Katusic, S.; Albers, P.; Kern, R.; Petrat, F. M.; Sastrawan, R.; Hore, S.; Hinsch, A.; Gutsch, A. *Sol. Energy Mater. Sol. Cells* **2006,** *90*, 1983-1999.

[3] Fujishima, A.; Honda, K. *Nature* **1972,** *238*, 37-38.

[4] Asahi, R.; Morikawa, T.; Ohwaki, T.; Aoki, K.; Taga, Y. *Science* **2001,** *293*, 269-271.

[5] Tricoli, A.; Righettoni, M.; Pratsinis, S. E. *Nanotechnology* **2009,** *20*, 315502.

[6] Herrmann, J. M. *Catal. Today* **1999,** *53*, 115-129.

[7] Chatterjee, D.; Dasgupta, S. *J. Photoch. Photobio. C* **2005,** *6*, 186-205.

[8] Hoffmann, M. R.; Martin, S. T.; Choi, W. Y.; Bahnemann, D. W. *Chem. Rev.* **1995,** *95*, 69-96.

[9] Linsebigler, A. L.; Lu, G. Q.; Yates, J. T. *Chem. Rev.* **1995,** *95*, 735-758.

[10] Di Valentin, C.; Finazzi, E.; Pacchioni, G.; Selloni, A.; Livraghi, S.; Paganini, M. C.; Giamello, E. *Chem. Phys.* **2007,** *339*, 44-56.

[11] Sato, S.; White, J. M. *Chem. Phys. Lett.* **1980,** *72*, 83-86.

[12] Fresno, F.; Coronado, J. A.; Tudela, D.; Soria, J. *Appl. Catal. B-Environ.* **2005,** *55*, 159-167.

[13] Oropeza, F. E.; Davies, B.; Palgrave, R. G.; Egdell, R. G. *Phys. Chem. Chem. Phys.* **2011,** *13*, 7882-7891.

[14] Paz, Y. In *Advances in Chemical Engineering*; Hugo, I. d. L., Benito Serrano, R., Eds.; Academic Press, 2009; Vol. 36; pp 289-336.

[15] Phillips, L. A.; Raupp, G. B. *J. Mol. Catal.* **1992,** *77*, 297-311.

[16] Anpo, M.; Chiba, K.; Tomonari, M.; Coluccia, S.; Che, M.; Fox, M. A. *B. Chem. Soc. JPN* **1991,** *64*, 543-551.

[17] Peral, J.; Ollis, D. F. *J. Catal.* **1992,** *136*, 554-565.

[18] Zakrzewska, K. *Thin Solid Films* **2001,** *391*, 229-238.

[19] Brattain, W. H.; Bardeen, J. *Bell Syst. Tech. J.* **1953,** *32*, 1-41.

[20] Brattain, W. H.; Garrett, C. G. B. *Physica* **1954,** *20*, 885-892.

[21] Snow, E. S.; Perkins, F. K.; Houser, E. J.; Badescu, S. C.; Reinecke, T. L. *Science* **2005,** *307*, 1942-1945.

[22] Yamazoe, N.; Miura, N. In *New Approaches in the Design of Gas Sensors*; Sberveglieri, G., Ed.; Kluwer Academic Publishers Group: Dordrecht, 1992; Vol.

[23] National Highway Traffic Safety Administration. Highway Saftey Programs; Conforming products list of screening devices to measure alcoholin bodily fluids. *Fed Regist.* **2009,** *74*, 66398-66400.

[24] Di Natale, C.; Macagnano, A.; Martinelli, E.; Paolesse, R.; D'Arcangelo, G.; Roscioni, C.; Finazzi-Agro, A.; D'Amico, A. *Biosens. Bioelectron.* **2003,** *18*, 1209-1218.

[25] Wang, L.; Teleki, A.; Pratsinis, S. E.; Gouma, P. I. *Chem. Mater.* **2008,** *20*, 4794-4796.

[26] Eranna, G.; Joshi, B. C.; Runthala, D. P.; Gupta, R. P. *Crit. Rev. Solid State* **2004,** *29*, 111-188.

[27] Korotcenkov, G. *Sensor. Actuat. B-Chem.* **2005,** *107*, 209-232.

[28] Han, X. G.; Jin, M. S.; Xie, S. F.; Kuang, Q.; Jiang, Z. Y.; Jiang, Y. Q.; Xie, Z. X.; Zheng, L. S. *Angew. Chem.-Int. Edit.* **2009,** *48*, 9180-9183.

[29] Tricoli, A.; Righettoni, M.; Teleki, A. *Angew. Chem.-Int. Edit.* **2010,** *49*, 7632-7659.

[30] Thiel, B.; Helbig, R. *J. Cryst. Growth* **1976,** *32*, 259-264.

[31] Cao, W. Q.; Duan, Y. X. *Clin. Chem.* **2006,** *52*, 800-811.

[32] Barsan, N.; Weimar, U. *J. Electroceram.* **2001,** *7*, 143-167.

[33] Barsan, N.; Weimar, U. *J. Phys-Condens. Mat.* **2003,** *15*, R813-R839.

[34] Righettoni, M.; Tricoli, A.; Pratsinis, S. E. *Anal. Chem.* **2010,** *82*, 3581-3587.

[35] Heiland, G.; Kohl, D. In *Chemical Sensor Technology*; Seiyama, T., Ed.; Kodansha Tokyo, 1988; Vol. 1; pp 24.

[36] Morrison, S. R. *The Chemical Physics of Surfaces*, 2nd ed.; Plenum: New York, 1990.

[37] Henrich, V. A., Cox, P. A. *The Surface Science of Metal Oxides*; Cambridge University Press: Cambridge, 1994.

[38] Grabow, L. C.; Gokhale, A. A.; Evans, S. T.; Dumesic, J. A.; Mavrikakis, M. *J. Phys. Chem. C* **2008,** *112*, 4608-4617.

[39] Zhang, J. L.; Vukmirovic, M. B.; Sasaki, K.; Nilekar, A. U.; Mavrikakis, M.; Adzic, R. R. *J. Am. Chem. Soc.* **2005,** *127*, 12480-12481.

[40] Ojeda, M.; Nabar, R.; Nilekar, A. U.; Ishikawa, A.; Mavrikakis, M.; Iglesia, E. *J. Catal.* **2010,** *272*, 287-297.

[41] Martínez, J. I.; Hansen, H. A.; Rossmeisl, J.; Nørskov, J. K. *Phys. Rev. B* **2009,** *79*, 045120.

[42] Sensato, F. R.; Custódio, R.; Calatayud, M.; Beltrán, A.; Andrés, J.; Sambrano, J. R.; Longo, E. *Surf. Sci.* **2002,** *511*, 408-420.

[43] Wendt, S.; Schaub, R.; Matthiesen, J.; Vestergaard, E. K.; Wahlström, E.; Rasmussen, M. D.; Thostrup, P.; Molina, L. M.; Lægsgaard, E.; Stensgaard, I.; Hammer, B.; Besenbacher, F. *Surf. Sci.* **2005,** *598*, 226-245.

[44] Evarestov, R. A.; Bandura, A. V.; Proskurov, E. V. *Phys. Status Solidi B* **2006,** *243*, 1823-1834.

[45] Ramamoorthy, M.; Vanderbilt, D.; Kingsmith, R. D. *Phys. Rev. B* **1994,** *49*, 16721-16727.

[46] Sensato, F. R.; Custódio, R.; Longo, E.; Beltrán, A.; Andrés, J. *Catal. Today* **2003,** *85*, 145-152.

[47] Hirata, T.; Ishioka, K.; Kitajima, M.; Doi, H. *Phys. Rev. B* **1996,** *53*, 8442-8448.

[48] Lindan, P. J. D. *Chem. Phys. Lett.* **2000,** *328*, 325-329.

[49] Bandura, A. V.; Kubicki, J. D.; Sofo, J. O. *J. Phys. Chem. B* **2008,** *112*, 11616-11624.

[50] Lindan, P. J. D.; Harrison, N. M.; Gillan, M. J. *Phys. Rev. Lett.* **1998,** *80*, 762-765.

[51] Lindan, P. J. D.; Zhang, C. J. *Phys. Rev. B* **2005,** *72*, 075439.

[52] Lippert, G.; Hutter, J.; Parrinello, M. *Mol. Phys.* **1997,** *92*, 477-487.

[53] Lippert, G.; Hutter, J.; Parrinello, M. *Theor. Chem. Acc.* **1999,** *103*, 124-140.

[54] VandeVondele, J.; Krack, M.; Mohamed, F.; Parrinello, M.; Chassaing, T.; Hutter, J. *Comput. Phys. Commun.* **2005,** *167*, 103-128.

[55] Goedecker, S.; Teter, M.; Hutter, J. *Phys. Rev. B* **1996,** *54*, 1703-1710.

[56] VandeVondele, J.; Hutter, J. *J. Chem. Phys.* **2007,** *127*, 114105.

[57] Perdew, J. P.; Burke, K.; Ernzerhof, M. *Phys. Rev. Lett.* **1996,** *77*, 3865-3868.

[58] Hahn, K. R.; Tricoli, A.; Santarossa, G.; Vargas, A.; Baiker, A. *Surf. Sci.* **2011,** *605*, 1476-1482.

[59] Goniakowski, J.; Gillan, M. J. *Surf. Sci.* **1996,** *350*, 145-158.

[60] Gercher, V. A.; Cox, D. F. *Surf. Sci.* **1995,** *322*, 177-184.

[61] Feibelman, P. J. *Science* **2002,** *295*, 99-102.

[62] Bates, S. P. *Surf. Sci.* **2002,** *512*, 29-36.

[63] Harris, L. A.; Quong, A. A. *Phys. Rev. Lett.* **2004,** *93*, 086105.

[64] Lindan, P. J. D.; Zhang, C. J. *Phys. Rev. Lett.* **2005,** *95*, -.

[65] Hugenschmidt, M. B.; Gamble, L.; Campbell, C. T. *Surf. Sci.* **1994,** *302*, 329-340.

[66] Henderson, M. A. *Surf. Sci.* **1996,** *355*, 151-166.

[67] Lin, W.; Zhang, Y. F.; Li, Y.; Ding, K. N.; Li, J. Q.; Xu, Y. J. *J. Chem. Phys.* **2006,** *124*, 054704.

[68] Long, R.; Dai, Y.; Huang, B. *J. Phys. Chem. C* **2009,** *113*, 650-653.

Table 1: Dissociative and associative H_2O binding energies at 1 ML and 1/12 ML coverage on SnO_2. All values are given in kJ/mol.

	dissociative	associative	mixed adsorption
1/12 ML	135.2	98.8	-
1 ML	145.2	112.0	137.8
reference	141[49]	113[a,49]	143[49]

[a] use of artificial constraints to obtain only associative H_2O adsorption

Table 2: Dissociative and associative H_2O binding energies at 1 ML and 1/12 ML coverage on TiO_2. All values are given in kJ/mol.

	dissociative	associative	mixed adsorption
1/12 ML	99.4	92.0 (89.5[a])	-
1 ML	60.3	78.7	75.4
	66[49]	83[49]	

[a] configuration parallel to surface (Fig. 5a,b)

Table 3: Bond length between Me_{5c} atoms and adsorbed OH_{term} groups (Me_{5c}-OH_{term}, Fig. 1b) and distance between OH groups (d_{root}, Fig. 1a) for dissociative H_2O adsorption at 1/12 ML coverage. All distances are given in Å. The increase of the standard deviation of d_{root} with the surface Ti-content reflects the irregularity of the surface.

	surf Ti-content [%]	Sn_{5c}-OH_{term}	Ti_{6c}-OH_{term}	d_{root}
SnO_2	0	2.02		2.36±0.002
$Sn_{1-x}Ti_xO_2$	12.5	2.02		2.35±0.013
	25	2.02		2.42±0.043
	37.5	2.01		2.45±0.040
	50	2.01		2.45±0.016
	66.7	2.01	1.84	2.64±0.175
	100		1.82	2.50±0.402
TiO_2	100		1.82	2.30±0.014

Table 4: Bond length between Me_{5c} atoms and adsorbed OH_{term} groups (Me_{5c}-OH_{term}, Fig. 1b) and distance between adjacent OH groups d_{root} and d_{term} (Fig. 1a) upon dissociative H_2O adsorption at 1 ML coverage. All distances are given in Å.

	surf Ti-content [%]	Sn_{5c}-OH_{term}	Ti_{6c}-OH_{term}	d_{root}	d_{term}
SnO_2	0	2.06		1.80	2.49
$Sn_{1-x}Ti_xO_2$	16.7	2.03		2.27	2.44
	33.3	2.02		2.49	2.35
	50	2.03		2.53	2.38
	66.7	2.03	1.86	2.30	2.40
	100		1.88	2.35	2.41
TiO_2	100		1.87	2.37	2.16

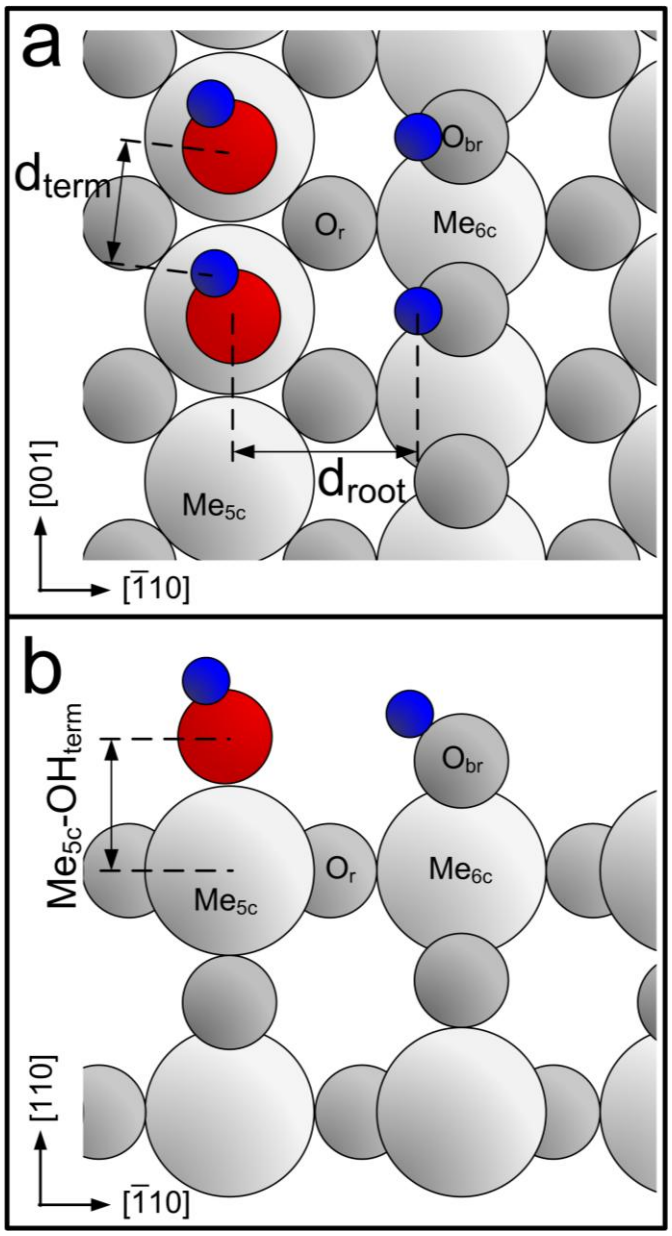

Figure 1

Top (a) and cross-sectional (b) schematic illustration of geometrical properties of dissociative H_2O adsorption on rutile (110). Large spheres indicate metal atoms (Sn or Ti), small gray spheres indicate O atoms of the (110) surface. Red spheres indicate O atoms of the adsorbing H_2O molecule and blue ones H atoms.

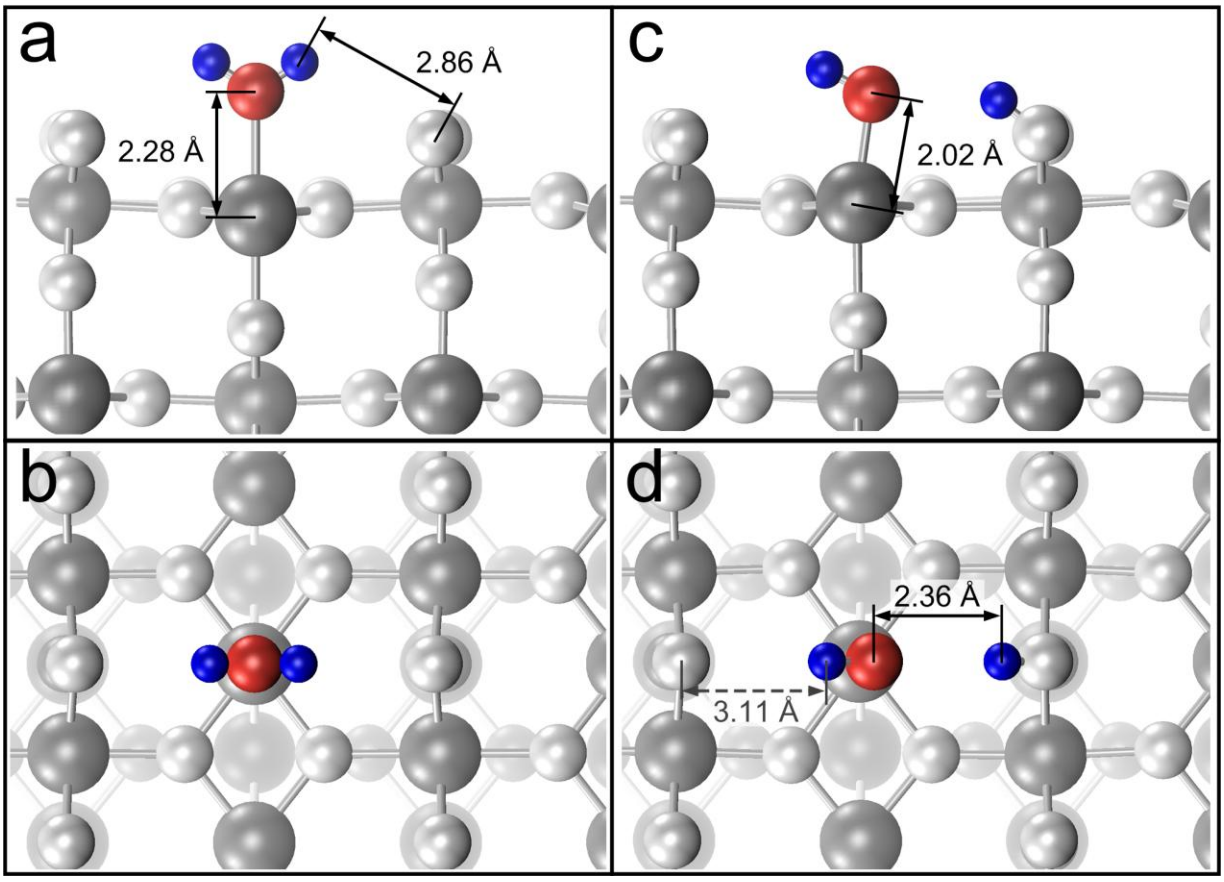

Figure 2

Cross-sectional (a,c) and top (b,d) view of stable configurations of isolated H_2O adsorbed associatively (a,b) and dissociatively (c,d) on SnO_2(110). The Sn-O bond length was remarkably smaller for dissociative adsorption (2.20 Å) than for associative one (2.28 Å) indicating stronger bonds. This was as well reflected in a higher binding energy of dissociative adsorption (Table 1).

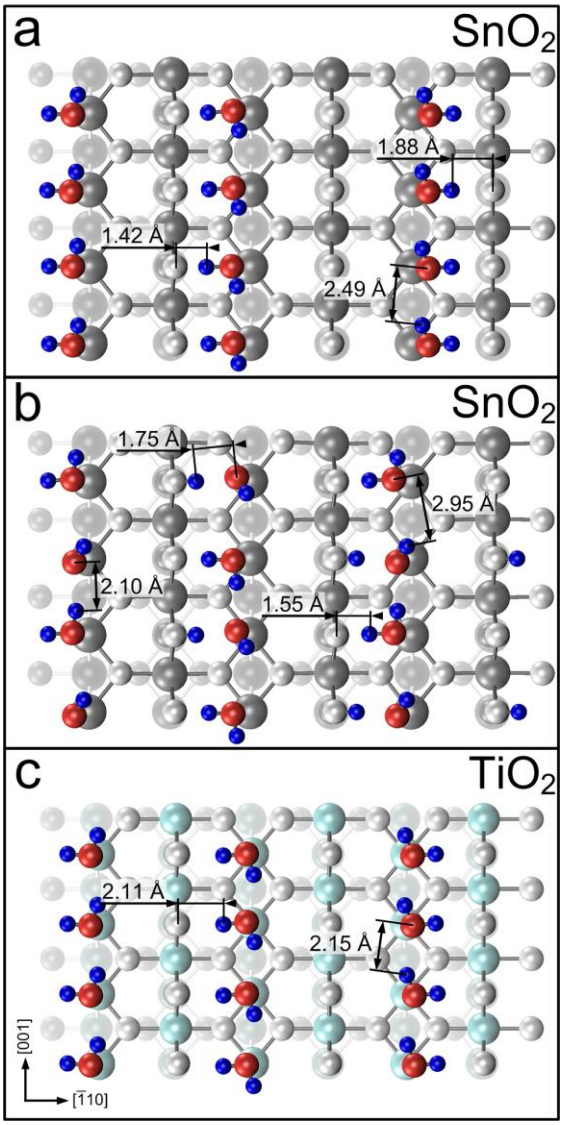

Figure 3

Top view of stable configurations for associative adsorption of H_2O at 1 ML coverage on SnO_2 (a) and TiO_2 (c). On SnO_2, when all molecules pointed into the same direction, H_2O spontaneously dissociated resulting in a mixed associative/dissociative adsorption state (b). Since the mixed adsorption state (b) also accounts for dissociative adsorption, the obtained energy was higher (137.8 kJ/mol, Table 1) than that for pure associative adsorption (112 kJ/mol). On TiO_2 (c), the H_2O molecules did not dissociate leading to pure associative adsorption even for a highly symmetric configuration with a binding energy of 78.7 kJ/mol. Sn: dark gray, Ti: cyan, surface O: light gray, O of H_2O: red, H: blue.

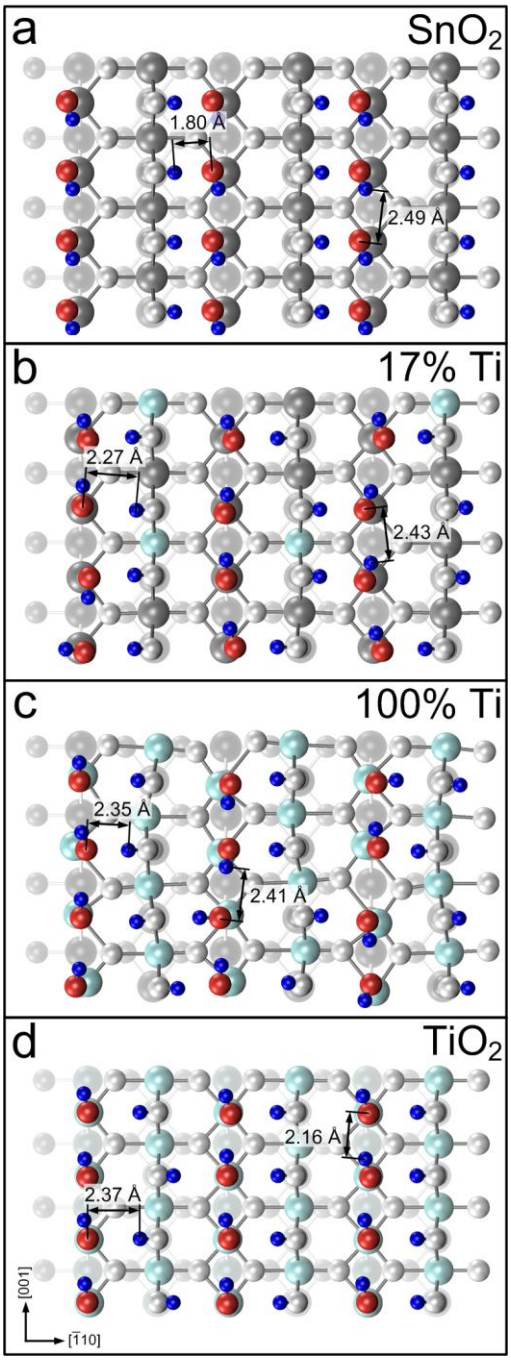

Figure 4

Top view of stable configurations of dissociative H_2O adsorption on SnO_2 (a), TiO_2 (d) and on $Sn_{1-x}Ti_xO_2$ with surface Ti-contents of 16.7% (b) and 100% (c) at 1 ML coverage. The calculated binding energies were:145.2 (a), 116.6 (b), 101.8 (c) and 60.3 kJ/mol (d). The inhomogeneity of the Ti-containing surfaces (b,c) led to an asymmetric configuration of dissociatively adsorbed H_2O. Despite their smaller lattice parameters, d_{root} was larger on the solid solutions and on pure TiO_2 than on pure SnO_2 indicating a loss of H-bonds.

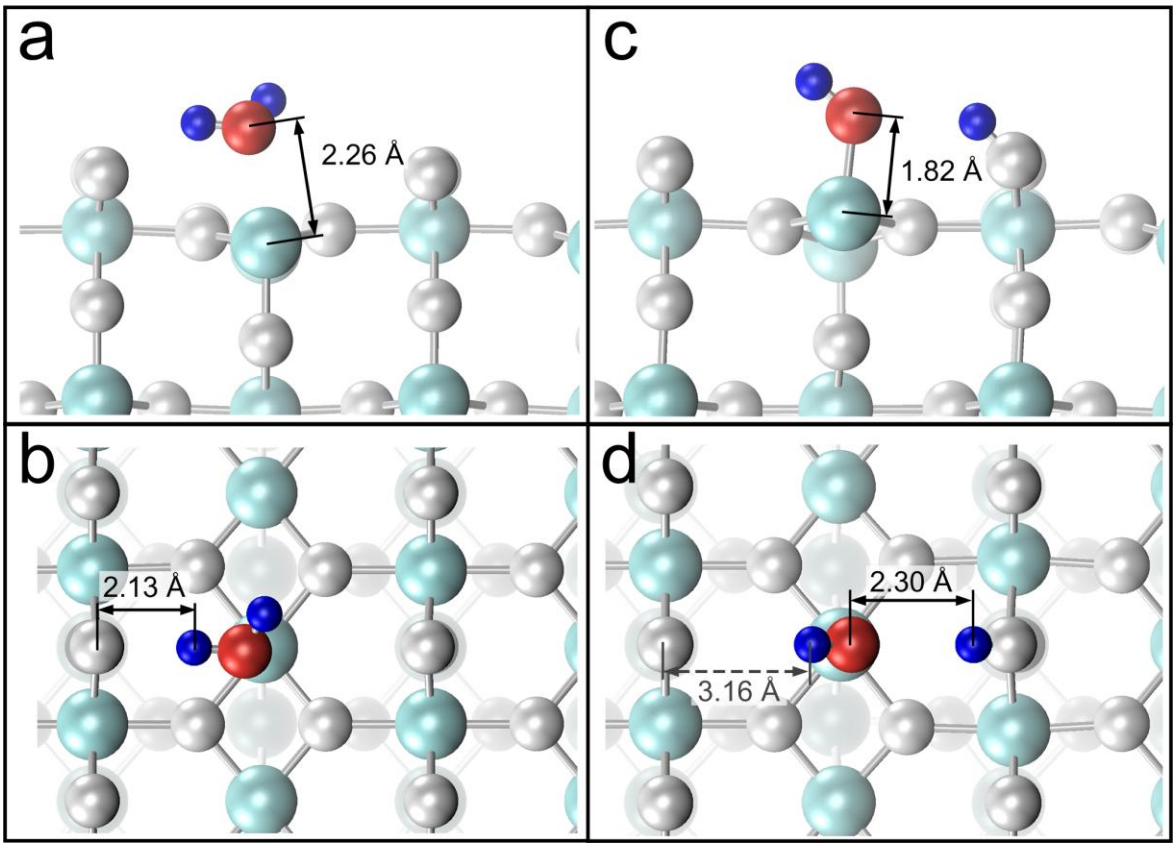

Figure 5

Cross-sectional (a,c) and top (b,d) view of stable configurations of isolated H_2O adsorbed associatively (a,b) and dissociatively (c,d) on TiO_2(110). A more stable state was found for associative adsorption in a perpendicular configuration similar to the one on SnO_2 (Fig. 2a,b). On TiO_2, the difference between the Ti-O bond length for associative and dissociative adsorption was even larger than on SnO_2, but less visible in the change of binding energy (Table 2).

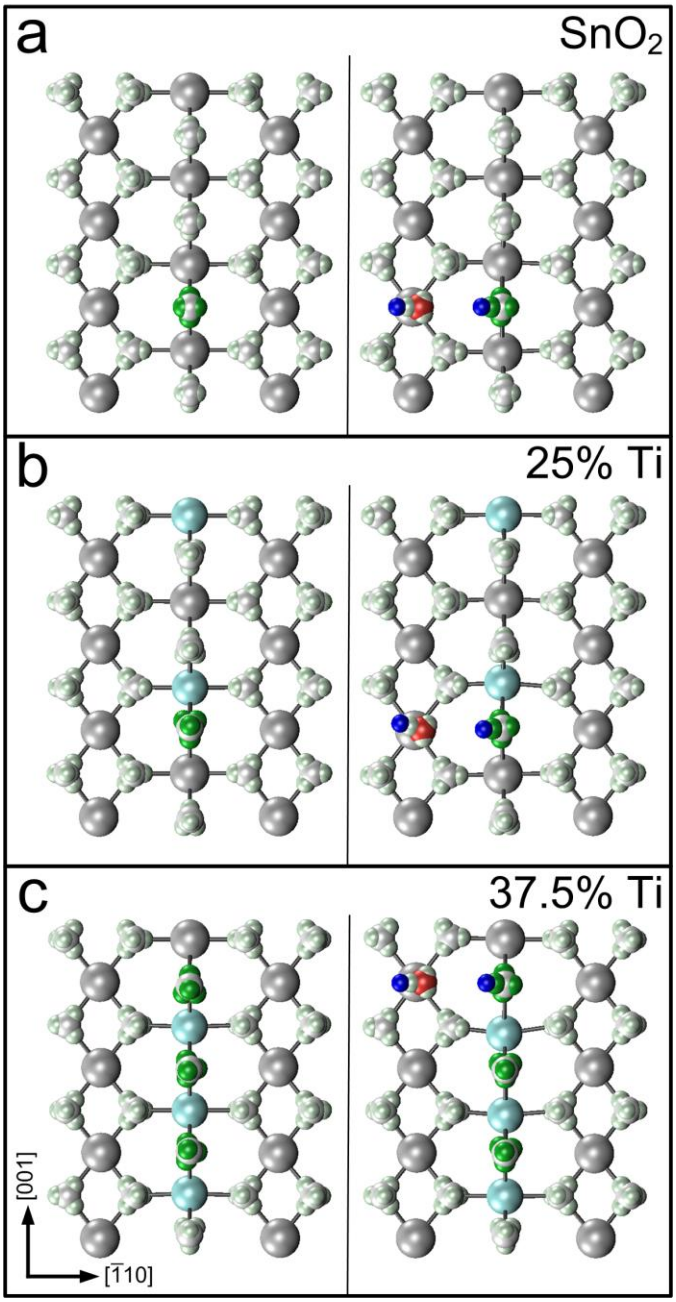

Figure 6

Top view of a section of the clean surface (left) of SnO_2 (a) and $Sn_{1-x}Ti_xO_2$ solid solutions with 25% (b) and 37.5% (c) surface Ti-content and after adsorption of one H_2O molecule (right side). Small spheres around O atoms indicate the center of Wannier functions. The centers important for H_2O adsorption are highlighted in green.

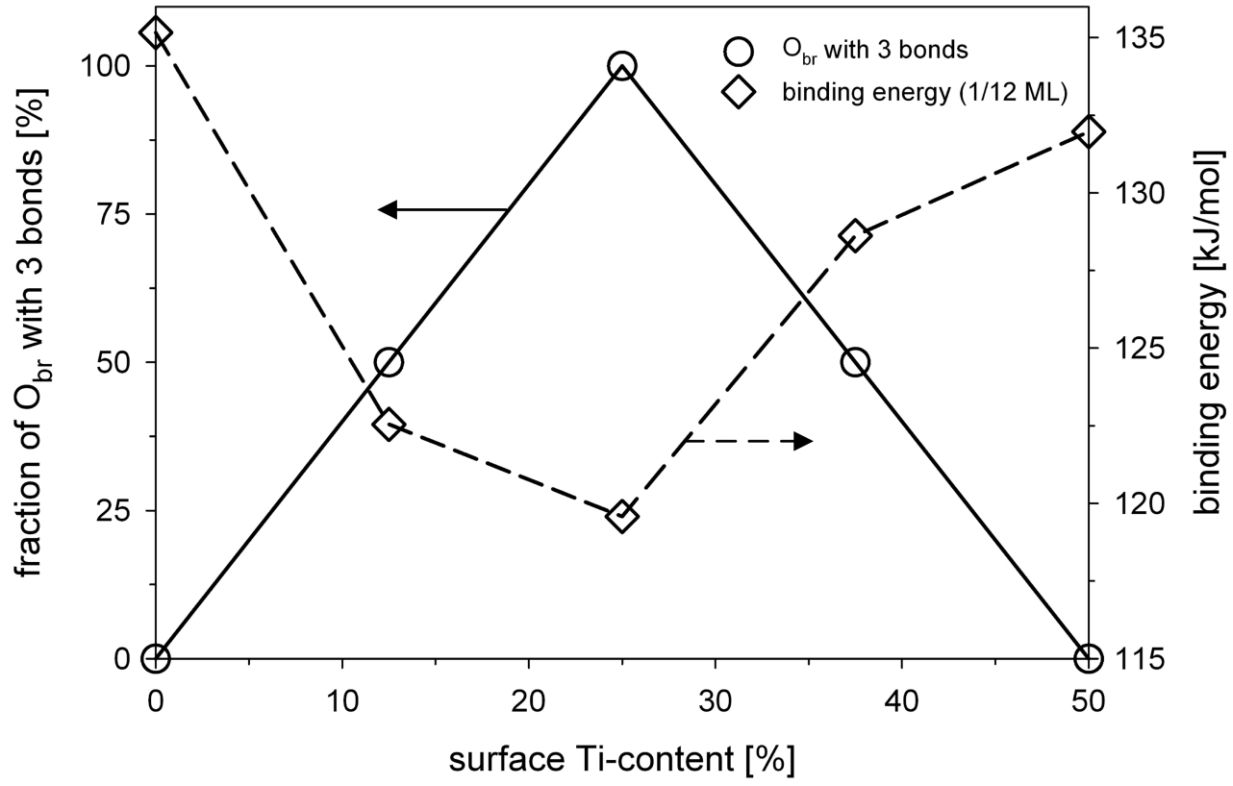

Figure 7

Fraction of O_{br} atoms on the (110) surface of $Sn_{1-x}Ti_xO_2$ solid solutions that form three bonds to neighboring Sn_{6c} or Ti_{6c} atoms as a function of the surface Ti-content (diamonds). When all 6c sites were occupied by the same type of metal atom (Sn for 0% and Ti for 50%), O_{br} atoms formed two bonds to the neighboring Me_{6c} atoms. However, when O_{br} was adjacent to an Sn_{6c} atom on one side and a Ti_{6c} atom on the other one, two bonds were formed to Ti and one to Sn. The number of O_{br} with such three bonds had a maximum at 25% surface Ti-content when Sn_{6c} and Ti_{6c} atoms were alternating. Upon H_2O adsorption, the third Ti_{6c}-O_{br} bond had to be broken resulting in an inverse behavior of the H_2O binding energy (triangles): the binding energy had a minimum at 25% surface Ti-content.

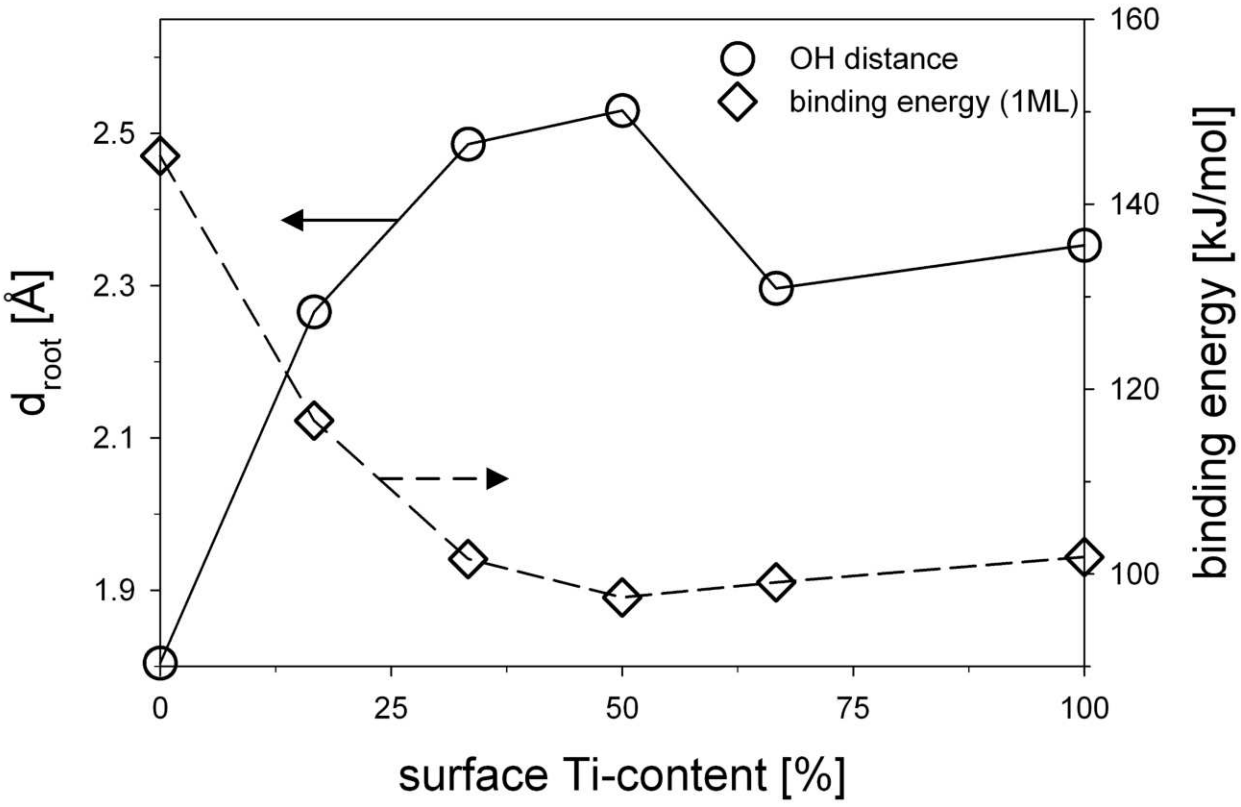

Figure 8

Change of d_{root} (circles) for 1 ML dissociative H_2O adsorption as a function of the surface Ti-content. Already at a surface Ti-content of 33 %, d_{root} drastically increased from 1.80 to 2.49 Å. At the same time, the H_2O binding energy (squares) decreased from 145.2 to 101.6 kJ/mol. This inverted trend suggests the presence of intermolecular H-bonds when d_{root} is small leading to higher binding energies.

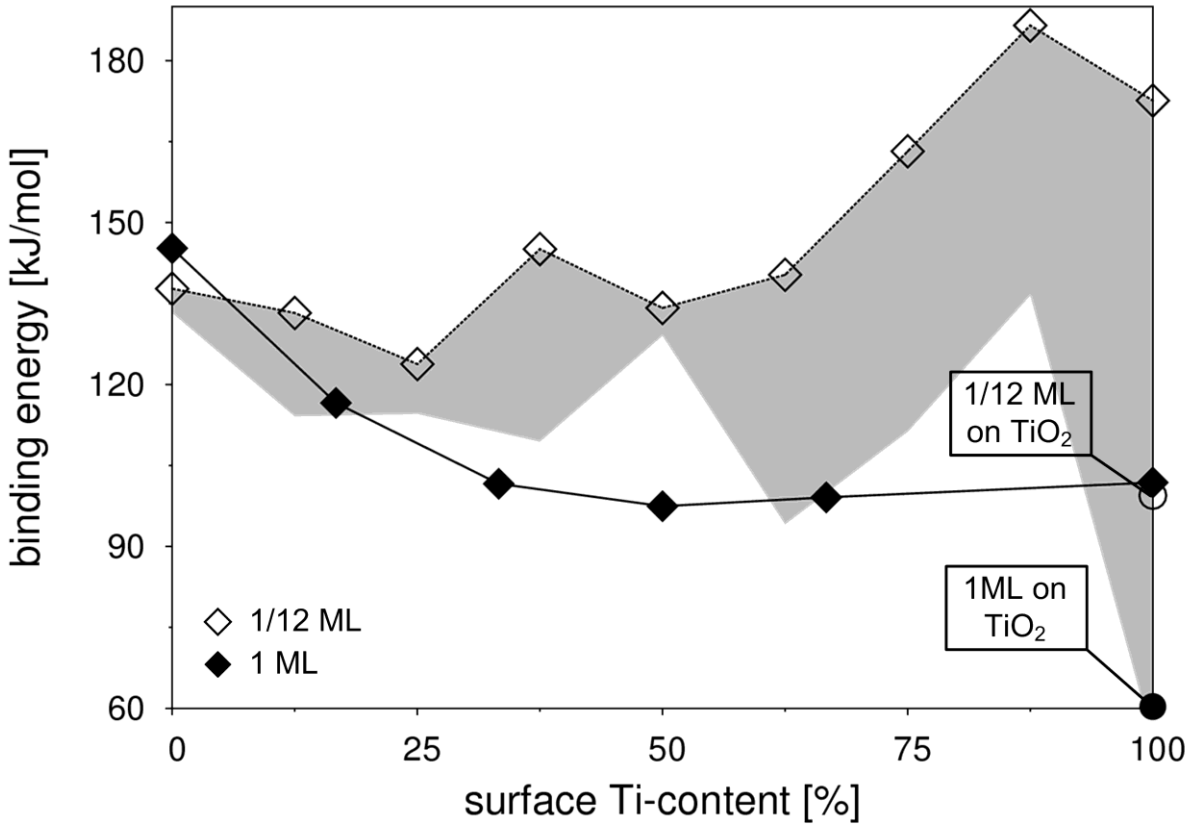

Figure 9

Maximum binding energy of dissociative H_2O adsorption on $Sn_{1-x}Ti_xO_2(110)$ surfaces at 1/12 ML (open diamonds) and average binding energy at 1 ML (filled diamonds) coverage as a function of the surface Ti-content. The gray area shows the range of different binding energies that were observed on different adsorption sites for each Ti-content. The 1/12 ML binding energy had a minimum at 25% surface Ti-content attributed to the maximum number of O_{br} atoms with three bonds to neighboring Me_{6c} atoms (Fig. 7). For higher surface Ti-contents the binding energy increased as well as the range of binding energies observed for each Ti-content. This was caused by a large degree of inhomogeneity of the surface structure. The 1 ML binding energy decreased drastically up to a surface Ti-content of 50%. Higher Ti-contents had hardly any effect on the binding energy.

TOC (table of contents only)